Atmos. Meas. Tech. Discuss., 7, 4229–4274, 2014
www.atmos-meas-tech-discuss.net/7/4229/2014/
doi:10.5194/amtd-7-4229-2014

Atmospheric Measurement Techniques Discussions
Open Access

Retrieval of three-dimensional small scale structures in upper tropospheric/lower stratospheric composition as measured by GLORIA

M. Kaufmann[1], J. Blank[1,*], T. Guggenmoser[1], J. Ungermann[1], A. Engel[7], M. Ern[1], F. Friedl-Vallon[2], D. Gerber[4], J. U. Grooss[1], G. Guenther[1], M. Höpfner[2], A. Kleinert[2], Th. Latzko[2], G. Maucher[2], T. Neubert[9], H. Nordmeyer[2], H. Oelhaf[2], F. Olschewski[3], J. Orphal[2], P. Preusse[1], H. Schlager[8], H. Schneider[9], D. Schuettemeyer[6], F. Stroh[1], O. Suminska-Ebersoldt[2], B. Vogel[1], C. M. Volk[3], W. Woiwode[2], and M. Riese[1]

[1]Institute of Energy and Climate Research, Stratosphere (IEK-7), Research Centre Jülich, 52425 Jülich, Germany
[2]Institute for Meteorology and Climate Research, Karlsruhe Institute of Technology, Karlsruhe, Germany
[3]Physics Department, University of Wuppertal, 42097 Wuppertal, Germany
[4]RAL Space, STFC Rutherford Appleton Laboratory, Harwell Oxford, Didcot, OX11 0QX, UK
[6]European Space Agency, Mission Science Division, 2200AG Noordwijk, the Netherlands

[7]Institute for Atmospheric and Environmental Sciences, Goethe University Frankfurt, 60438 Frankfurt/Main, Germany
[8]German Aerospace Center, Institute of Atmospheric Physics, Atmospheric trace gases, 82234 Oberpfaffenhofen-Wessling, Germany
[9]Central Institute of Engineering, Electronics and Analytics (ZEA-2) – Electronic Systems, Research Centre Jülich, Jülich, Germany
[*]now at: Google Inc., Dublin, Ireland

Received: 17 March 2014 – Accepted: 1 April 2014 – Published: 29 April 2014

Correspondence to: M. Kaufmann (m.kaufmann@fz-juelich.de)

Published by Copernicus Publications on behalf of the European Geosciences Union.

Abstract

The three-dimensional quantification of small scale processes in the upper troposphere and lower stratosphere is one of the challenges of current atmospheric research and requires the development of new measurement strategies. This work presents first results from the newly developed Gimballed Limb Observer for Radiance Imaging of the Atmosphere (GLORIA) obtained during the ESSenCe and TACTS/ESMVal aircraft campaigns. The focus of this work is on the so-called dynamics mode data characterized by a medium spectral and a very high spatial resolution. The retrieval strategy for the derivation of two- and three-dimensional constituent fields in the upper troposphere and lower stratosphere is presented. Uncertainties of the main retrieval targets (temperature, O_3, HNO_3 and CFC-12) and their spatial resolution are discussed. During ESSenCe, high resolution two-dimensional cross-sections have been obtained. Comparisons to collocated remote-sensing and in-situ data indicate a good agreement between the data sets. During TACTS/ESMVal a tomographic flight pattern to sense an intrusion of stratospheric air deep into the troposphere has been performed. This filament could be reconstructed with an unprecedented spatial resolution of better than 500 m vertically and 20 km × 20 km horizontally.

1 Introduction

The upper troposphere and lower stratosphere gained increasing attention in recent years due to their importance in the climate system (Solomon et al., 2007; Riese et al., 2012). Quantifying the structure and chemical composition to understand the underlying physical processes are current topics of atmospheric research. The quantification of small scale structures and dynamical processes is a key topic for the understanding of this atmospheric region (Gettelman et al., 2011), because cross-tropopause transport and mixing around jet streams give an important contribution to stratosphere-troposphere exchange (e.g., Manney et al., 2011; Seo and Bowman, 2002; Olsen et al., 2008) and affect the mixing layers above the tropopause (e.g., Hoor et al., 2002).

Satellite borne limb observations have enhanced our understanding of the three-dimensional chemical structure and large-scale dynamics of the middle atmosphere significantly in recent years. Our knowledge of small scale structures is, however, primarily based on in-situ observations by means of research aircraft and high altitude balloons. Airborne limb-emission sensors such as CRISTA-NF (CRyogenic Infrared Spectrometers and Telescopes for the Atmosphere – New Frontiers; Weigel et al., 2012; Ungermann et al., 2013) and MIPAS-STR (Michelson Interferometer for Passive Atmospheric Sounding – STRatospheric Aircraft, Piesch et al., 1996; Woiwode et al., 2012) complemented the satellite and in-situ data with their high spatial sampling in two dimensions (vertical and along the flight track).

The quantification of small scale processes in all three dimensions requires the development of new instruments and new measurement strategies. Ungermann et al. (2010) presented a new approach to obtain trace gas filaments and temperature fluctuations by means of airborne remote sounding utilizing tomographic reconstruction techniques. The two key factors for this measurement strategy are closed or nearly closed flight paths (diameter of a few hundred kilometers) and the ability to make measurements from different viewing angles with respect to the aircraft position.

The Gimballed Limb Observer for Radiance Imaging of the Atmosphere (GLORIA; Riese et al., 2014; Friedl-Vallon et al., 2014) is an instrument newly developed to deliver data for such kind of tomographic reconstruction. It can measure images of mid infrared limb emission spectra within a few seconds and has the capability to pan its line of sight from 48 to 118° with respect to the aircraft nose.

This work describes results from the first two deployments of the GLORIA instrument, namely during ESSenCe (ESa Sounder Campaign; Kaufmann et al., 2013) and during the TACTS/ESMVal campaign (TACTS: Transport and composition in the upper troposphere/lower most stratosphere, ESMVal: Earth System Model Validation). The former campaign was conducted to perform a first in-flight testing of the GLORIA instrument

AMTD
7, 4229–4274, 2014

and to verify the GLORIA retrieval products. In the latter campaign, several closed flight paths have been performed to allow for the application of tomographic reconstruction techniques to real GLORIA measurements for the first time.

The outline of this paper is as followed: after a short description of the GLORIA instrument (Sect. 2), we describe the retrieval strategy for the GLORIA so-called dynamics mode measurements (Sect. 3) including a short review of the forward- and inverse model. Section 4 gives an overview about the ESSenCe campaign and presents first GLORIA measurements including a discussion of their uncertainties, vertical resolution, and a comparison with collocated measurements and simulations. First tomographic measurements of a filamentary structure during the TACTS/ESMVal campaign are presented in Sect. 5.

2 GLORIA instrument

GLORIA is an infrared limb sounder which combines the high horizontal resolution of a nadir sounder (tens of km) with the altitude resolution provided by a limb-sounding instrument. The purpose of GLORIA is to measure temperature and composition in the upper troposphere/lower stratosphere at high spatial resolution (Riese et al., 2014). This is achieved by mounting an imaging Michelson interferometer with a high resolution two-dimensional infrared detector in a gimbal which allows to point and stabilize the instrument in azimuthal, elevational and image rotation direction (Friedl-Vallon et al., 2014; Maucher et al., 2014). It is designed to be deployed on board different research aircraft, namely the Russian high altitude research aircraft M55 Geophysica and the German High Altitude and LOng Range (HALO) research aircraft.

GLORIA is able to measure infrared limb or nadir emissions between 780 cm^{-1} and 1400 cm^{-1}. The limb images cover a vertical field of view of 0.8° to −3.3° with respect to the horizontal, the latter corresponding to a lower tangent altitude of about 4 km. The field of view can be pointed about 10° upward as a quasi deep space view and into two large area blackbodies for radiometric calibration (Olschewski et al., 2013).

Tomographic measurements are performed in the so called dynamics mode. In this mode, GLORIA operates at low optical path differences to obtain more spectra at a given time. During ESSenCe GLORIA recorded spectra at a maximum optical path difference of 1.6 cm in 2.8 s for a pair of forward/backward spectra, yielding a spectral sampling of 0.3125 cm^{-1}. During TACTS/ESMVal dynamics mode spectra were recorded at a maximum optical path difference of 0.8 cm in 2 s for a pair of forward/backward spectra, yielding a spectral sampling of 0.625 cm^{-1}. Another measurement mode is the so called chemistry mode with a spectral sampling of 0.0625 cm^{-1} and 12 s measurement time. GLORIA data recorded in chemistry mode are analyzed by Woiwode et al. (2014). Individual GLORIA images contain 128 × 48 pixel/spectra. The horizontal resolution of the detector array is used to analyze and filter cloud fractions. After filtering, the spectra are averaged horizontally on a 128 × 1 grid for further processing. Different viewing angles of the same air mass are obtained by pointing the instrument from 48 to 118° (4° steps) with respect to the aircraft nose in a short time frame. The data obtained in this way can be combined and processed in a tomographic way to get a three-dimensional picture of the atmosphere.

3 Data processing

When operating the GLORIA instrument during a field measurement, raw interferograms and house keeping data are written to a mass storage for later processing. The data rate is about 1 Gbit s^{-1}. In the laboratory, this data is processed in several steps, including different calibration procedures and the retrieval of atmospheric temperature, trace gases, etc. These steps and the corresponding data level products are described below.

AMTD
7, 4229–4274, 2014

3.1 Level 0 and Level 1

The Level 0 and Level 1 processing transforms the measured raw interferograms into radiometrically and spectrally calibrated spectra. The core of the Level 0 processing is the resampling of the interferograms. The raw interferograms are sampled on a time-equidistant grid. Before Fourier transformation, they have to be interpolated onto a space-equidistant grid, taking velocity variations of the interferometer drive into account. The Level 0 processing also includes a quality check of the data, spike detection and correction, non-linearity correction, correction of phase errors, and the spectral calibration. The Level 1 processing comprises the Fourier transform converting the interferograms to complex spectra and the radiometric calibration. Calibration spectra are generated from blackbody and quasi deep space measurements using a two-point calibration. Details about the Level 0 and Level 1 processing of GLORIA data are given in Kleinert et al. (2014).

3.2 Level 2

Level 2 processing encompasses the derivation of atmospheric or instrumental parameters from calibrated radiance measurements. This is performed in an iterative way by minimizing the difference between a forward model mapping an atmospheric state to radiances as they would have been observed by the instrument and real GLORIA measurements. This minimization is performed by the so-called inversion model.

3.2.1 Forward modeling

The forward model consists of a radiative transfer and an instrument model. The radiative transfer model is based on a combination of the emissivity growth approximation (EGA; Gordley and Russell, 1981) and the Curtis–Godson approximation (CGA; Curtis, 1952; Godson, 1953). Both methods are based on pre-calculated emissivities of homogeneous gas cells for a variety of atmospheric conditions and pre-defined spectral

AMTD
7, 4229–4274, 2014

ranges. The spectral ranges are either individual spectral points or integrated spectral windows combining several spectral points (Riese et al., 1997, 1999). The optical paths have been calculated by means of the line-by-line Reference Forward Model (RFM, Dudhia, 2000) utilizing the HITRAN-2012 spectral database (Rothman et al., 2013). The speed up of this method is up to three orders of magnitude in comparison to a line-by-line model and the uncertainties arising from the approximations are generally less than one percent (Marshall et al., 1994; Francis et al., 2006; Ungermann et al., 2013).

The second part of the forward model is the instrument model. It maps various line of sight radiances onto the detector array. To consider field of view effects, several line of sight radiances are typically combined to simulate one or more detector pixel.

The retrieval of atmospheric quantities requires the calculation of the Jacobian of the forward model (see Sect. 3.2.2). This is done by algorithmic differentiation (Lotz et al., 2011; Ungermann et al., 2011), which is highly efficient in our case, because the computational costs for calculating the Jacobian matrix are only a constant multiple of a single execution of the forward model.

3.2.2 Inverse modeling

The reconstruction of an atmospheric state compatible with a sequence of GLORIA measurements is a non-linear inversion problem. This is solved by minimizing a cost function σ_y describing the difference between the forward model F: $\mathbb{R}^n \rightarrow \mathbb{R}^m$ of an atmospheric state $\boldsymbol{x} \in \mathbb{R}^n$ (temperature, trace gas abundance, etc.) and the radiance measurement $\boldsymbol{y} \in \mathbb{R}^m$:

$$\sigma_y = (F(\boldsymbol{x}) - \boldsymbol{y})^T \mathbf{S}_\epsilon^{-1} (F(\boldsymbol{x}) - \boldsymbol{y}) \tag{1}$$

The difference is weighted by the inverse measurement error/error covariance matrix $\mathbf{S}_\epsilon^{-1}$. In most cases, the solution is not unique and/or under-constrained. Therefore it

Discussion Paper | Discussion Paper | Discussion Paper | Discussion Paper |

AMTD

7, 4229–4274, 2014

Retrieval of three-dimensional small scale structures

M. Kaufmann et al.

has proven useful to add a regularization term to the cost function:

$$\sigma_x = (\boldsymbol{x} - \boldsymbol{x}_\mathrm{a})^T \mathbf{L}^T \mathbf{L} (\boldsymbol{x} - \boldsymbol{x}_\mathrm{a}) \quad (2)$$

In our case, **L** the is a Tikhonov type matrix applying difference operators of zero and first order (Twomey, 1977). A zero order Tikhonov regularization constrains the absolute value, while the first order minimizes the derivative in order to smooth the solution. $\boldsymbol{x}_\mathrm{a}$ describes a-priori information about the atmospheric state. $\boldsymbol{x}$ and $\boldsymbol{x}_\mathrm{a}$ may also contain parameters of the instrument model, such as a radiance offset. The definition of the a-priori data and the regularization matrix **L** depends on the atmospheric conditions and the instrument performance and is described later (Sect. 4.3.1).

The overall cost function is then $\sigma = \sigma_y + \sigma_x$, which is minimized using a truncated Quasi–Newton minimizer. For three-dimensional tomographic retrieval setups, the size of the state- and measurement space is rather large ($n \approx 10^7$, $m \approx 10^6$), and sparse matrix structures for storage and iterative methods for solving linear equation systems are applied. The typical memory and computing requirements for such a setup are demanding and require the utilization of a parallel computer. The retrieval of the tomographic flight discussed in Sect. 5 was performed on 6 computing nodes with 48 CPU cores and 384 GiB main memory.

4 ESSenCe

4.1 Overview

GLORIA was deployed during the ESSenCe campaign for the first time. The main objective of this campaign was the in-flight testing of the GLORIA instrument under stratospheric conditions and the first verification/validation of the GLORIA retrieval products (Kaufmann et al., 2013).

Most favorable conditions for such a test campaign are cloud-free conditions utilizing an aircraft carrier which can fly as high as possible into the stratosphere. For this

AMTD
7, 4229–4274, 2014

purpose, the Russian M55 Geophysica was chosen, which has a ceiling altitude of about 21 km. The aircraft is highly flexible in terms of operations, ground weather as well as stratospheric conditions. The campaign base was Kiruna in northern Sweden.

The first part of the ESSenCe campaign consisted of ground based measurements inside and outside of the hangar Arena Arctica to assure the interaction of all subsystems of the GLORIA instrument after transport and final integration. Several certification and calibration measurements were conducted, including electromagnetic tests of GLORIA when mounted on Geophysica.

The second part of the campaign consisted of flights with full instrumentation under stratospheric conditions. Flight patterns were planned such that the functionality and performance of GLORIA could be tested under all major conditions that are expected during later research flights. This includes particularly electromagnetic compatibility considerations (under flight conditions), the thermal behavior of the sensor and the gimbal frame, the detector and instrument optics cooling system, the pointing system, and the interferometer control system.

The dynamic conditions of the Arctic upper troposphere and lower stratosphere during the ESSenCe campaign were mostly undisturbed. At the beginning of the campaign in early December 2011 a low pressure system over the Norwegian Sea was slowly approaching Scandinavia. East of this low, mid-latitudinal air was moved polewards, thereby being lifted isentropically. Connected to the lows frontal system high clouds appeared south of this tongue of air (Fig. 1, blue lines). On the western rim of the low pressure system air from the lower stratosphere was descending deep into the troposphere, coiling up cyclonically. A few days later, the polar vortex strengthened and showed very low core temperatures with values well below 190 K in the lower stratosphere. Due to large-scale disturbances the vortex center was moved towards the European sector and air from the vortex edge was moved polewards over Siberia, thus forming a broad intrusion of air with low potential vorticity reaching from Siberia across the north pole to the Norwegian Sea.

4.2 GLORIA operations

Two GLORIA flights were performed during ESSenCe. Flight 1 took place on 11 December, 2011, 11:00–15:00 UTC, and Flight 2 on 16 December, 2011, 14:00–17:50 UTC, respectively. Although the instrument encountered some technical problems, partly related to the extremely cold temperatures in the polar vortex, GLORIA took nominal atmospheric measurements including calibration for more than one hour during each flight. During Flight 1, all measurements were taken in chemistry mode while during Flight 2, both chemistry and dynamics mode measurements were performed.

Due to interferometer slide velocity variations during the first flight, these data were utilized for engineering purposes, only. The functionality of the gimbal frame was partly lost in both flights after 1–2 h of flight time. For the remaining flight time it was not possible to compensate the image rotation anymore. The loss of pointing and image stabilization capabilities impacts data quality significantly such that Level 0 to Level 2 processing was restricted to the first measurement period of the 2nd flight. The flight path of the Geophysica aircraft and GLORIA instrument operations during the 2nd flight are illustrated in Fig. 1.

During both ESSenCe flights one of the internal blackbodies and quasi deep space spectra are used for a two point radiometric calibration. The latter exhibit remnants of atmospheric radiation, namely signatures of CO_2 below 750 cm^{-1}, O_3 around 1050 cm^{-1}, and CH_4 and N_2O around 1300 cm^{-1}, which affect the radiometric accuracy. These spectral windows are not used in the retrieval.

A typical GLORIA raw data image is illustrated in Fig. 2. It demonstrates the ability of the instrument to resolve spatial structures in the atmosphere as low as 150 m in horizontal and vertical direction. Constantly high signals in the lower two thirds of the image indicate gray body emissions from clouds or aerosol layers at these altitudes. In contrast to cloud sensing, the observation and quantification of trace gas filaments or temperature fluctuations does not require a horizontal resolution as provided by

AMTD
7, 4229–4274, 2014

individual GLORIA pixel. Therefore only the mean value for each detector row is used in the subsequent processing. No averaging in the vertical direction of the image is applied. Broken pixel (deviation of more than two times the standard deviation from the line average) or pixel pointing to clouds are removed. Entire detector rows are ignored if more than 75 % of the pixels are marked as broken or cloudy. Weighting of individual pixels is based on the noise analysis of blackbody spectra. Typical GLORIA dynamics mode spectra for the binned data are illustrated in Fig. 3. The ro-vibrational emission lines of CO_2 at 792 cm^{-1}, CFC-11 at 850 cm^{-1}, and HNO_3 at 890 cm^{-1} are clearly visible in the data.

Figure 4 illustrates the horizontal scan pattern of the GLORIA dynamics mode measurements during ESSenCe. As stated above, the line of sight is panned from 48° to 118° with respect to the airplane nose. GLORIA dynamics mode data were recorded from 14:58 to 15:10 UTC yielding to 121 individual images at about 2200 spectral points.

4.3 GLORIA Level 2 data analysis

4.3.1 Retrieval setup

The retrieval setup for GLORIA depends on the instrument performance and atmospheric conditions. It consists of the choice of spectral windows utilized for the radiative transfer forward model, the a priori and regularization parameters utilized in the constrained global fit method, and the error covariance matrix of the measurements.

The selection of appropriate spectral windows for the GLORIA dynamics mode retrieval is non-trivial, because the spectral resolution of this mode does not allow to separate individual trace gas emission lines. In addition, the radiometric calibration procedure utilizing “quasi” deep space spectra (in contrast to “real” deep space spectra as observed from a satellite) causes a non-uniform error pattern in the wavelength domain. Therefore the selection of spectral windows is performed by an automatic algorithm maximizing the information gain obtained by the measurements. The figure

AMTD
7, 4229–4274, 2014

of merit for information gain is determined by the instrumental uncertainties and the a priori knowledge (Kullback and Leibler, 1951). This selection is performed by a newly developed genetic algorithm optimizing the spectral window size and position simultaneously (Blank, 2013). In contrast to previous work (von Clarmann and Echle, 1998; Dudhia et al., 2002), this method does not require pre-selected broader spectral ranges and is able to optimize several spectral windows simultaneously. The latter is most relevant here due to the limited spectral resolution of the GLORIA dynamics mode measurements.

For ESSenCe, the main retrieval targets are temperature, O_3, HNO_3 and CFC-12. The spectral windows as selected by the genetic algorithm to retrieve these quantities are illustrated in Fig. 5. There are twice as many spectral windows than main retrieval targets to consider cloud/aerosol effects as well as other contaminant gases. A priori data for the constrained global fit are taken from the MIPAS reference atmospheres (Remedios et al., 2007). Some species (such as CO_2) were updated to 2011 conditions. Pressure and temperature data were taken from the ECMWF ERA-Interim data set (Dee et al., 2011). The penalty of zero order regularization (Eq. 2) was suppressed by a factor of three in comparison to an optimal estimation method assuming the standard deviations of the MIPAS climatology. For temperature and pressure, an uncertainty of 3 K and 1 % is assumed, respectively. Weighting factors for the first order regularization in the vertical direction are inversely proportional to the standard deviations of the MIPAS climatology multiplied by a characteristic length scale of 0.25 km for temperature and CFC-12 and 1 km for O_3 and HNO_3, respectively. The horizontal weighting factor is 100 km for all species.

The characterization of the GLORIA measurement error covariance matrix is work in progress. The main source of uncertainty is instrument noise, approximated by a diagonal matrix assuming an uncertainty of 25 nW/(cm^{-2} sr cm^{-1}) and 2 %, respectively. The transportation and mounting of the GLORIA instrument into the aircraft, as well as thermal stress during a research flight may cause a misalignment between the GLORIA attitude control system and the interferometer's line of sight. Therefore, it is mandatory

AMTD
7, 4229–4274, 2014

to verify the vertical pointing of the instrument and apply some corrections, if necessary. This is done by simulating the CO_2 Q-branch emissions at 792.5 cm^{-1} adopting ECMWF temperature data for the entire flight. Assuming that the real atmosphere during a research flight has a mean temperature similar to ECMWF data, a single elevation angle correction is retrieved. In the case of ESSenCe Flight 2 this correction is 0.1955°. Since the dominant uncertainties of the resulting line of sight elevation angles are not expected to change during the flight, small and medium scale structures in atmospheric temperature data can still be resolved by the measurement. The effect of the remaining pointing uncertainty of 0.023° is considered in the error budget of the retrieval targets (see Sect. 4.3.2).

4.3.2 Results, uncertainties and comparison to other measurements

Typical limb radiance altitude profiles for a few spectral windows are illustrated in Fig. 6. The intensities are generally increasing towards lower altitudes, as expected. The dynamical range given by maximum and minimum observed radiances in the considered spectral range varies between 50 % and 500 % for tangent altitudes between 9 km and 17 km, respectively.

Corresponding retrieval results for the main targets of the GLORIA dynamics mode are illustrated in Fig. 7. The most prominent feature in the retrieved quantities is a pronounced enhancement of O_3 and HNO_3 around an altitude of 14 km, which may point to a filamentary structure in the stratosphere. This enhancement extends several hundred kilometers horizontally, as indicated by the two-dimensional cross-sections measured by GLORIA (Fig. 8). The uncertainties of HNO_3 and O_3 (Fig. 9) are in the order of 0.25 ppbv and 0.1 ppbv, respectively and are clearly dominated by detector noise. This means, that the trace gas enhancement at 14 km is significant, whereas the small scale structures below this altitude are within the noise error. The vertical resolution (Fig. 10) is about 500 m for HNO_3 and O_3, and somewhat worse for temperature (750 m) and CFC-12 (600–1400 m). The vertical gradient of CFC-12 dynamics mode data as well as its (comparatively low) vertical resolution does not allow to resolve the filament at

AMTD
7, 4229–4274, 2014

14 km, whereas the high vertical resolution of O_3 and HNO_3 should give a realistic picture of this structure.

To validate these GLORIA measurements the retrieved data are compared to several other instruments. These are the two limb emission sounders mounted on the same airplane as GLORIA, namely the MIPAS-STR (Woiwode et al., 2012) and MARSCHALS (Millimetre-wave Airborne Receivers for Spectroscopic Characterization in Atmospheric Limb Sounding, Castelli et al., 2013) instruments. Furthermore, two in situ datasets obtained during the ascent and descent of the second ESSenCe flight are used for the comparison, namely measurements of the Whole Atmosphere Sampler (WAS; Laube et al., 2013) and the High Altitude Gas AnalyzeR (HAGAR; Volk et al., 2000; Werner et al., 2010) datasets. In addition, GLORIA measurements are compared to the satellite borne limb emission measurements of MIPAS (Fischer et al., 2007) on ESA's Environmental Satellite (Envisat) and the Earth Observing System (EOS) Microwave Limb Sounder (EOS-MLS, data version v03.33; Froidevaux et al., 2008) on NASA's EOS AURA satellite. The MIPAS data were derived with the retrieval processor of the Karlsruhe Institute of Technology; data version is V5R_O3_221 and V5R_HNO3_221 for ozone and HNO_3 (von Clarmann et al., 2009) and V5R_CFC-11_221 for CFC-11 (Kellmann et al., 2012). Finally, the GLORIA data are compared to simulations of the Chemical Lagrangian Model of the Stratosphere (CLaMS; Konopka et al., 2007; Grooß et al., 2014, and references therein). CLaMS runs with full stratospheric chemistry (including heterogeneous chemistry and sedimentation) and is driven by ERA-Interim reanalysis data (for the detailed model setup, see Vogel et al., 2014). The simulations cover an altitude range from the surface up to the 900 K potential temperature with a horizontal resolution of approximately 100 km and a maximum vertical resolution of about 400 m around the tropopause. The simulations were initialized on 1 November 2011 (for ESSenCe) and on 1 May 2012 (for the TACTS/ESMVal campaign), respectively, using satellite measurements and tracer tracer correlations following Grooß et al. (2014).

AMTD
7, 4229–4274, 2014

The mismatch in distance between the comparison data and GLORIA's tangent points is typically a few hundred kilometers (Fig. 4). Since this is larger than the spatial extent of the GLORIA dynamics mode measurements and since the atmospheric scene is relatively homogeneous in the horizontal direction (Fig. 8), the entire dynamics mode sequence from 14:58 to 15:10 UTC was averaged for comparison with the other data sets.

The satellite instruments' vertical profiles exhibit a much coarser altitude resolution than the GLORIA data. This effect is taken into account by convolving the GLORIA data $\boldsymbol{x}_{\text{gloria}}$ with the averaging kernel of these instruments ($\mathrm{A}_{\text{mipas}}$ and A_{mls}) considering the respective a priori data ($\boldsymbol{x}^{\text{apr}}_{\text{mipas}}$ and $\boldsymbol{x}^{\text{apr}}_{\text{mls}}$):

$$\boldsymbol{x}^{\text{conv}}_{\text{gloria}} = \boldsymbol{x}^{\text{apr}}_{\text{mipas/mls}} + \mathrm{A}_{\text{mipas/mls}} \left(\boldsymbol{x}_{\text{gloria}} - \boldsymbol{x}^{\text{apr}}_{\text{mipas/mls}} \right)$$

Figures 11–13 show a comparison of GLORIA retrieval results with the different data sets described above. The left panel of these figures illustrates the data "as it is", and the right panel shows differences between GLORIA and the other data sets, where the effect of the averaging kernels was taken into account for the calculation of the differences. It is obvious, that the effect of the averaging kernel is rather large for the comparison with the satellite instruments, because the vertical resolution of the satellite data sets is several kilometers in the lower stratosphere.

GLORIA O_3 data show an excellent agreement with MARSCHALS data, which were recorded a few minutes (14:52–14:56 UTC) before GLORIA dynamics mode measurements. MARSCHALS O_3 abundance was retrieved from the Band B data (297–305 GHz). Differences between the two datasets are a few percent and smaller than the combined error bars. Most notable is the observation of the O_3 enhancement at 14 km in both datasets. Technical improvements of the MARSCHALS instrument and a new retrieval setup (Gerber, 2014) allowed the derivation of such a fine structure from MARSCHALS data for the first time. O_3 observations of MIPAS-STR exhibit similar absolute values, but the local enhancement at 14 km is not resolved due to the

AMTD
7, 4229–4274, 2014

coarser altitude resolution of this dataset. Differences to the satellite borne datasets of EOS-MLS are typically less than 15 % and somewhat larger for MIPAS-Envisat, but both datasets cannot resolve the ozone enhancement at 14 km due to their broad averaging kernels. CLaMS model simulations do not show this localized enhancement either, which is consistent with the non-existence of this structure in the ERA-interim data at a resolution of $1^\circ \times 1^\circ$ as utilized for this model run. However, modified potential vorticity data (Müller and Günther, 2003) based upon ECMWF operational analyzes at a much higher spatial resolution ($0.1^\circ \times 0.1^\circ$, not shown here) reveals increased values at an altitude of 13.5 km at the location of the GLORIA measurements. This indicates that two different air masses get close together and model simulations at higher spatial resolution are needed to resolve such structures.

Mixing ratios of HNO_3 measured from GLORIA and MIPAS-STR show similar values at most altitudes as well – differences are typically less than 15 %, except for the 14 km region, where GLORIA data is enhanced by more than 1 ppbv. MIPAS-Envisat HNO_3 values (spatial separation 350–550 km) are 20–50 % larger than the other two datasets, which may be due to the differences in the tangent point location and viewing geometry.

For CFC-12, GLORIA data shows a small high bias of about 5 % in the entire altitude region in comparison to collocated MIPAS-STR data. This bias is also observed in comparison to the CFC-12 data of the WAS and HAGAR in-situ instruments measured during the ascent and descent of the aircraft. CLaMS results are in good agreement with the in-situ measurements. Although this difference between GLORIA and the in-situ or model data is within the error margins of the GLORIA instrument, it may point so some instrumental issues to be solved in future missions.

AMTD
7, 4229–4274, 2014

Retrieval of three-dimensional small scale structures

M. Kaufmann et al.

Title Page
Abstract Introduction
Conclusions References
Tables Figures
◀ ▶
Back Close
Full Screen / Esc
Printer-friendly Version
Interactive Discussion

5 The TACTS/ESMVal campaign

5.1 Overview

The second deployment of GLORIA was during the TACTS/ESMVal campaign in September 2012. This campaign was conducted by means of the new German High Altitude and LOng Range Research Aircraft. It covered a broad geographical region from Spitsbergen at high northern latitudes to Antarctica in the South and from western Africa in the West to the Arabian Sea in the East. The main scientific objective of the TACTS campaign is the measurement of the composition of the lowermost stratosphere during the period from summer to autumn to quantify the transport and mixing in the upper troposphere/lower stratosphere in the vicinity of the subtropical jet. The ESMVal campaign aimed to provide a large set of constituent, aerosol, and cloud data for the validation and improvement of chemistry-climate models. TACTS/ESMVal yielded nearly 90 h of GLORIA measurements at different atmospheric situations and measurement modes.

The aim of this section is to show some preliminary results regarding the three-dimensional reconstruction of a filament, thereby demonstrating the outstanding capabilities of GLORIA to resolve such small scale structures in all three dimensions.

5.2 GLORIA measurements

Since the implementation during ESSenCe the GLORIA instrument was subject to several improvements. Problems with the gimbal frame and with some interferometer components have been solved and instrument configurations have been optimized. The spectral resolution of the dynamics mode during TACTS/ESMVal has been halved compared to ESSenCe.

During TACTS/ESMVal, the aircraft flew on several closed loop flight tracks to test GLORIA's capabilities to sound the atmosphere tomographically. One of these closed path flight tracks took place on 13 September 2012 south of Africa at the edge of the antarctic polar vortex (Fig. 14). This region is characterized by strong gradients in potential vorticity, ozone, and HNO_3 mixing ratios. At the edge of the polar vortex, HALO performed a hexagonal flight track, such that the GLORIA lines of sight are directed to the center of the hexagon. At this location (45° S, 20° E) the horizontal winds are sheared and tilted as a consequence of a distortion of the jet stream at lower altitudes (Fig. 15). Wind speeds are in the order of $45\,\mathrm{m\,s^{-1}}$.

To retrieve the atmospheric composition within the air volume contained by the hexagon, an appropriate atmospheric grid was defined. The size of the grid cells is based on the vertical and horizontal field of view of the GLORIA instrument, namely 125 m in the vertical and 7.5 km in the horizontal direction, respectively, resulting in about 2×10^6 individual cells. The size of the grid cells is increasing towards the boundaries of the air-volume.

The horizontal and vertical regularization applied to the retrieval targets is similar to ESSenCe, as is the selection of spectral windows. The reduced spectral resolution and uncertainties in the instrument calibration led to the elimination of a few spectral windows describing the aerosol background and some "secondary" gases such as PAN or $ClONO_2$, which cannot be retrieved with high confidence for this atmospheric situation. The most relevant difference to ESSenCe is the omission of the spectral window at $845\,\mathrm{cm^{-1}}$ showing strong CFC-11 emissions, which turned out to be contaminated by instrument emissions from the optical window of GLORIA (Kleinert et al., 2014). Cloud indices (Spang et al., 2004) observed during the hexagonal flight were 4–6 between 9 km and 14 km, indicating an almost cloud free atmosphere.

Retrieved temperature and constituent fields exhibit a pronounced intrusion of stratospheric air into the troposphere at about 45° S, 20° E (Fig. 16). This intrusion is observed between an altitude of 12.5 km and 14.5 km and extends about 500 m vertically. The horizontal extent is about 200 km and non-uniform in the longitudinal direction. Its stratospheric nature is indicated by enhanced HNO_3 and O_3 – at least by a factor of two compared to the air parcels just below or above the filament. This enhancement is significantly larger than the uncertainty of these species. Temperature data does not

AMTD
7, 4229–4274, 2014

show this filamentary structure and varies by less than 2 K in the vicinity of this structure. CFC-12 does not show a pronounced structure as well due to its weak vertical gradient at these altitudes.

Using three-dimensional tomography the horizontal resolution is about 20 km in the core of the measured atmospheric region (Fig. 17). In this region, each atmospheric grid cell is measured from at least 4 different directions. The vertical resolution of the atmospheric fields is 200–300 m and somewhat larger than for the data obtained from the linear flight tracks during ESSenCe due to the increased instrument performance of GLORIA during the TACTS/ESMVal campaign. Since the calculation of retrieval diagnostics such as averaging kernel and spatial resolution is computationally very demanding (it breaks the sparsity of the computational problem; see, e.g., Ungermann et al., 2010), this information has not been calculated for all atmospheric grids cells considered in the retrieval.

A preliminary comparison to the CLaMS simulation for this flight (Fig. 14) indicates that the model resolution of 100 km (horizontally) is in turn not sufficient to resolve this intrusion of air as observed by the tomographic sounding.

6 Conclusions

The first two deployments of GLORIA demonstrated the readiness of this instrument to measure upper tropospheric/lower stratospheric composition at high spatial resolution. The retrieval of temperature, O_3, HNO_3 and CFC-12 flagged no major problems, except for a small bias in CFC-12 data. Increased effort in the radiometric calibration procedure will reduce this bias in future data versions. During ESSenCe GLORIA already demonstrated its ability to measure intrusions of stratospheric air on vertical scales as low as a few hundred meters. However, the outstanding capability of the GLORIA instrument can only come into full effect when the airplane carrier flies a closed path around the air volume to be observed as it was performed several times during the TACTS/ESMVal campaign. In these cases, GLORIA data can provide three-dimensional constituent data at horizontal scales as low as a few tens of kilometers.

The major improvement to conventional limb sounders not applying tomographic inversion techniques is the reduction of the horizontal (line of sight) smearing of these instruments. This is particularly important, if the small scale structure to be observed is smaller than the horizontal averaging kernel or if it is not co-aligned with the line of sight. Figure 18 illustrates this effect in the case of the filament observed during TACTS/ESMVal. The plot on the right hand side shows the three-dimensional reconstruction of the HNO_3 filament (Fig. 16), sampled at the tangent points of each segment of the hexagon. The plot on the left hand side shows the result of a conventional one-dimensional retrieval approach assuming horizontal homogeneity along the instrument's line of sight. The quality of the match between the retrieved structures and the tilt of the filament is dependent on a good alignment of the line of sight of a given segment and that of the filament. An example of a good match is found at 13:50 UTC; whereas a worse case is found at 13:40 UTC. Since the orientation of the filament is generally not known a-priori, the tomographic data gives a more realistic picture of the structure.

GLORIA represents the first airborne realization of the infrared limb imaging technique. The capabilities of this technique were also studied for application from a low Earth-orbit satellite (ESA, 2012). For the satellite payload, the lines of sight of the imager are in flight direction so that trace gas fields can be obtained with a similar horizontal resolution as for the tomographic reconstruction of airborne GLORIA dynamics mode data as presented in this study.

Acknowledgements. We acknowledge financial support by the German Helmholtz society (ATMO, ATMONSYS), by the European Space Agency/Mission Science Division (ESSenCe), and the Deutsche Forschungsgemeinschaft in the priority program 1294 "Atmospheric and Earth system research with the High Altitude and Long Range Research Aircraft (HALO)". GLORIA retrieval activities were supported under the DFG project RASGLO (HALO-SPP 1294/Ka 2324/1-2) and flight planning by CLaMS model forecasts under the DFG project LASSO (HALO-SPP 1294/GR 3786).

We thank all members of the GLORIA instrument team for their large efforts in the development of the GLORIA instrument and the conduction of the ESSenCe and TACTS/ESMVal campaigns.

We acknowledge the contribution of L. Hoffmann and S. Griessbach (both at Research Center Juelich), G. Geppert (now at Max Planck Institute for Meteorology), Ch. Kaliczinsky (Wuppertal University), and K. Leppkes and J. Lotz (both at RWTH Aachen) for their contribution to the development of the retrieval code.

We like to thank Th. Roeckmann (Institute for Marine and Atmospheric Research Utrecht, Utrecht University) and J. Laube (School of Environmental Sciences, University of East Anglia) for providing the Whole Atmosphere Sampler data.

We thank J. Wintel (Physics Department, University of Wuppertal) for the measurement of the High Altitude Gas AnalyzeR data.

We thank the satellite group at IMK-ASF for providing the MIPAS data, the MLS team for providing EOS-MLS data, and the CLaMS team for assisting the flight planning.

Finally, we like to acknowledge the open source community for the development of programming and visualization tools such as scientific python, matplotlib or swig.

The service charges for this open access publication have been covered by a Research Centre of the Helmholtz Association.

References

Blank, J.: Tomographic Retrieval of Atmospheric Trace Gases Observed by GLORIA, Ph.D. thesis, Bergische Universität Wuppertal, 2013. 4241

Castelli, E., M. Dinelli, B., Del Bianco, S., Gerber, D., Moyna, B. P., Siddans, R., Kerridge, B. J., and Cortesi, U.: Measurement of the Arctic UTLS composition in presence of clouds using millimetre-wave heterodyne spectroscopy, Atmos. Meas. Tech., 6, 2683–2701, doi:10.5194/amt-6-2683-2013, 2013. 4243

Curtis, A. R.: Discussion of “A statistical model for water vapour absorption” by R. M. Goody, Q. J. Roy. Meteor. Soc., 78, 638–640, 1952. 4235

Dee, D. P., Uppala, S. M., Simmons, A. J., Berrisford, P., Poli, P., Kobayashi, S., Andrae, U., Balmaseda, M. A., Balsamo, G., Bauer, P., Bechtold, P., Beljaars, A. C. M., van de Berg, L., Bidlot, J., Bormann, N., Delsol, C., Dragani, R., Fuentes, M., Geer, A. J., Haimberger, L., Healy, S. B., Hersbach, H., Hólm, E. V., Isaksen, L., Kållberg, P., Köhler, M., Matricardi, M., McNally, A. P., Monge-Sanz, B. M., Morcrette, J.-J., Park, B.-K., Peubey, C., de Rosnay, P., Tavolato, C., Thépaut, J.-N., and Vitart, F.: The ERA-Interim reanalysis: configuration and performance of the data assimilation system, Q. J. Roy. Meteor. Soc., 137, 553–597, 2011. 4241

Dudhia, A.: Michelson Interferometer for Passive Atmospheric Sounding (MIPAS) Reference Forward Model (RFM), Software User's Manual, available at: http://eodg.atm.ox.ac.uk/RFM/sum/ (last access: 25 April 2014), 2000. 4236

Dudhia, A., Jay, V. L., and Rodgers, C. D.: Microwindow selection for high-spectral-resolution sounders, Appl. Optics, 41, 3665–3673, doi:10.1364/AO.41.003665, 2002. 4241

ESA: Report for Mission Selection: PREMIER, volume SP-1324/3, ESA Communication Production Office, Noordwijk, the Netherlands, 2012. 4249

Fischer, H., Birk, M., Blom, C., Carli, B., Carlotti, M., von Clarmann, T., Delbouille, L., Dudhia, A., Ehhalt, D., Endemann, M., Flaud, J. M., Gessner, R., Kleinert, A., Koopman, R., Langen, J., López-Puertas, M., Mosner, P., Nett, H., Oelhaf, H., Perron, G., Remedios, J., Ridolfi, M., Stiller, G., and Zander, R.: MIPAS: an instrument for atmospheric and climate research, Atmos. Chem. Phys., 8, 2151–2188, doi:10.5194/acp-8-2151-2008, 2008. 4243

Francis, G. L., Edwards, D. P., Lambert, A., Halvorson, C. M., Lee-Taylor, J. M., and Gille, J. C.: Forward modeling and radiative transfer for the NASA EOS-Aura High Resolution Dynamics Limb Sounder (HIRDLS) instrument, J. Geophys. Res.-Atmos., 111, D13301, doi:10.1029/2005JD006270, 2006. 4236

Friedl-Vallon, F., Gulde, T., Hase, F., Kleinert, A., Kulessa, T., Maucher, G., Neubert, T., Olschewski, F., Piesch, C., Preusse, P., Rongen, H., Sartorius, C., Schneider, H., Schönfeld, A., Tan, V., Bayer, N., Blank, J., Dapp, R., Ebersoldt, A., Fischer, H., Graf, F., Guggenmoser, T., Höpfner, M., Kaufmann, M., Kretschmer, E., Latzko, T., Nordmeyer, H., Oelhaf, H., Orphal, J., Riese, M., Schardt, G., Schillings, J., Sha, M. K., Suminska-Ebersoldt, O., and Ungermann, J.: Instrument concept of the imaging Fourier transform spectrometer GLORIA, Atmos. Meas. Tech. Discuss., 7, 2301–2337, doi:10.5194/amtd-7-2301-2014, 2014. 4232, 4233

AMTD
7, 4229–4274, 2014

Froidevaux, L., Jiang, Y. B., Lambert, A., Livesey, N. J., Read, W. G., Waters, J. W., Browell, E. V., Hair, J. W., Avery, M. A., McGee, T. J., Twigg, L. W., Sumnicht, G. K., Jucks, K. W., Margitan, J. J., Sen, B., Stachnik, R. A., Toon, G. C., Bernath, P. F., Boone, C. D., Walker, K. A., Filipiak, M. J., Harwood, R. S., Fuller, R. A., Manney, G. L., Schwartz, M. J., Daffer, W. H., Drouin, B. J., Cofield, R. E., Cuddy, D. T., Jarnot, R. F., Knosp, B. W., Perun, V. S., Snyder, W. V., Stek, P. C., Thurstans, R. P., and Wagner, P. A.: Validation of Aura Microwave Limb Sounder stratospheric ozone measurements, J. Geophys. Res.-Atmos., 113, D15S20, doi:10.1029/2007JD008771, 2008. 4243

Gerber, D.: MARSCHALS measurements during ESSenCe, Atmos. Meas. Tech. Discuss., in preparation, 2014. 4244

Gettelman, A., Hoor, P., Pan, L. L., Randel, W. J., Hegglin, M. I., and Birner, T.: The extratropical upper troposphere and lower stratosphere, Rev. Geophys., 49, RG3003, doi:10.1029/2011RG000355, 2011. 4231

Godson, W. L.: The evaluation of infra-red radiative fluxes due to atmospheric water vapour, Q. J. Roy. Meteor. Soc., 79, 367–379, 1953. 4235

Gordley, L. L. and Russell, J. M.: Rapid inversion of limb radiance data using an emissivity growth approximation, Appl. Optics, 20, 807–813, 1981. 4235

Grooß, J.-U., Engel, I., Borrmann, S., Frey, W., Günther, G., Hoyle, C. R., Kivi, R., Luo, B. P., Molleker, S., Peter, T., Pitts, M. C., Schlager, H., Stiller, G., Vömel, H., Walker, K. A., and Müller, R.: Nitric acid trihydrate nucleation and denitrification in the Arctic stratosphere, Atmos. Chem. Phys., 14, 1055–1073, doi:10.5194/acp-14-1055-2014, 2014. 4243

Hoor, P., Fischer, H., Lange, L., Lelieveld, J., and Brunner, D.: Seasonal variations of a mixing layer in the lowermost stratosphere as identified by the CO–O_3 correlation from in situ measurements, J. Geophys. Res.-Atmos., 107, ACL1-1–ACL1-11, 2002. 4232

Kaufmann, M., Blank, J., Friedl-Vallon, F., Gerber, D., Guggenmoser, T., Höpfner, M., Kleinert, A., Sha, M. K., Oelhaf, H., Riese, M., Suminska-Ebersoldt, O., Woiwode, W., Siddans, R., Kerridge, B., Moyna, B., Rea, S., and Oldfield, M.: Technical Assistance for the Deployment of Airborne Limbsounders During ESSenCe, Technical Report, European Space Agency, 2013. 4232, 4237

Kellmann, S., von Clarmann, T., Stiller, G. P., Eckert, E., Glatthor, N., Höpfner, M., Kiefer, M., Orphal, J., Funke, B., Grabowski, U., Linden, A., Dutton, G. S., and Elkins, J. W.: Global CFC-11 (CCl_3F) and CFC-12 (CCl_2F_2) measurements with the Michelson Interferometer for

AMTD
7, 4229–4274, 2014
Retrieval of three-dimensional small scale structures
M. Kaufmann et al.

Passive Atmospheric Sounding (MIPAS): retrieval, climatologies and trends, Atmos. Chem. Phys., 12, 11857–11875, doi:10.5194/acp-12-11857-2012, 2012. 4243

Kleinert, A., Friedl-Vallon, F., Guggenmoser, T., Höpfner, M., Neubert, T., Ribalda, R., Sha, M. K., Ungermann, J., Blank, J., Ebersoldt, A., Kretschmer, E., Latzko, T., Oelhaf, H., Olschewski, F., and Preusse, P.: Level 0 to 1 processing of the imaging Fourier transform spectrometer GLORIA: generation of radiometrically and spectrally calibrated spectra, Atmos. Meas. Tech. Discuss., 7, 2827–2878, doi:10.5194/amtd-7-2827-2014, 2014. 4235, 4247

Konopka, P., Günther, G., Müller, R., dos Santos, F. H. S., Schiller, C., Ravegnani, F., Ulanovsky, A., Schlager, H., Volk, C. M., Viciani, S., Pan, L. L., McKenna, D.-S., and Riese, M.: Contribution of mixing to upward transport across the tropical tropopause layer (TTL), Atmos. Chem. Phys., 7, 3285–3308, doi:10.5194/acp-7-3285-2007, 2007. 4243

Kullback, S. and Leibler, R. A.: On information and sufficiency, Ann. Math. Stat., 22, 79–86, 1951. 4241

Laube, J. C., Keil, A., Bönisch, H., Engel, A., Röckmann, T., Volk, C. M., and Sturges, W. T.: Observation-based assessment of stratospheric fractional release, lifetimes, and ozone depletion potentials of ten important source gases, Atmos. Chem. Phys., 13, 2779–2791, doi:10.5194/acp-13-2779-2013, 2013. 4243

Lotz, J., Naumann, U., and Ungermann, J.: Efficient Discrete Adjoint Computation in a Spectral Simulation Code, Technical Report AIB-2011-05, RWTH Aachen and Forschungszentrum Jülich, 2011. 4236

Manney, G. L., Hegglin, M. I., Daffer, W. H., Santee, M. L., Ray, E. A., Pawson, S., Schwartz, M. J., Boone, C. D., Froidevaux, L., Livesey, N. J., Read, W. G., and Walker, K. A.: Jet characterization in the upper troposphere/lower stratosphere (UTLS): applications to climatology and transport studies, Atmos. Chem. Phys., 11, 6115–6137, doi:10.5194/acp-11-6115-2011, 2011. 4231

Marshall, B. T., Gordley, L. L., and Chu, D. A.: BANDPAK: algorithms for modeling broadband transmission and radiance, J. Quant. Spectrosc. Ra., 52, 581–599, 1994. 4236

Maucher, G., Bayer, N., Friedl-Vallon, F., Graf, F., Kulessa, T., Latzko, T., Neubert, T., Preusse, P., Schneider, H., Schönfeld, A., and Streit, M.: The pointing system of GLORIA, Atmos. Meas. Tech. Discuss., in preparation, 2014. 4233

Müller, R. and Günther, G.: A generalized form of Lait's modified potential vorticity, J. Atmos. Sci., 60, 2229–2237, 2003. 4245

AMTD

7, 4229–4274, 2014

Nash, E. R., Newman, P. A., Rosenfield, J. E., and Schoeberl, M. R.: An objective determination of the polar vortex using Ertel's potential vorticity, J. Geophys. Res., 101, 9471–9478, 1996. 4270

Olschewski, F., Ebersoldt, A., Friedl-Vallon, F., Gutschwager, B., Hollandt, J., Kleinert, A., Monte, C., Piesch, C., Preusse, P., Rolf, C., Steffens, P., and Koppmann, R.: The in-flight blackbody calibration system for the GLORIA interferometer on board an airborne research platform, Atmos. Meas. Tech., 6, 3067–3082, doi:10.5194/amt-6-3067-2013, 2013. 4233

Olsen, M. A., Douglass, A. R., Newman, P. A., Gille, J. C., Nardi, B., Yudin, V. A., Kinnison, D. E., and Khosravi, R.: HIRDLS observations and simulation of a lower stratospheric intrusion of tropical air to high latitudes, Geophys. Res. Lett., 35, L21813, doi:10.1029/2008GL035514, 2008. 4232

Piesch, C., Gulde, T., Sartorius, C., Friedl-Vallon, F., Seefeldner, M., Wölfel, M., Blom, C., and Fischer, H.: Design of a MIPAS instrument for high-altitude aircraft, presented at the Second International Airborne Remote Sensing Conference and Exhibition, Vol. 24, 27, 1996. 4232

Remedios, J. J., Leigh, R. J., Waterfall, A. M., Moore, D. P., Sembhi, H., Parkes, I., Greenhough, J., Chipperfield, M.P., and Hauglustaine, D.: MIPAS reference atmospheres and comparisons to V4.61/V4.62 MIPAS level 2 geophysical data sets, Atmos. Chem. Phys. Discuss., 7, 9973–10017, doi:10.5194/acpd-7-9973-2007, 2007. 4241

Riese, M., Preusse, P., Spang, R., Ern, M., Jarisch, M., Grossmann, U., and Offermann, D.: Measurements of trace gases by the CRyogenic Infrared Spectrometers and Telescopes for the Atmosphere (CRISTA) experiment, Adv. Space Res., 19, 563–566, 1997. 4236

Riese, M., Tie, X., Brasseur, G., and Offermann, D.: Three-dimensional simulation of stratospheric trace gas distributions measured by CRISTA, J. Geophys. Res.-Atmos., 104, 16419–16435, 1999. 4236

Riese, M., Ploeger, F., Rap, A., Vogel, B., Konopka, P., Dameris, M., and Forster, P.: Impact of uncertainties in atmospheric mixing on simulated UTLS composition and related radiative effects, J. Geophys. Res., 117, D16305, doi:10.1029/2012JD017751, 2012. 4231

Riese, M., Oelhaf, H., Preusse, P., Blank, J., Ern, M., Friedl-Vallon, F., Fischer, H., Guggenmoser, T., Höpfner, M., Hoor, P., Kaufmann, M., Orphal, J., Plöger, F., Spang, R., Suminska-Ebersoldt, O., Ungermann, J., Vogel, B., and Woiwode, W.: Gimballed Limb Observer for Radiance Imaging of the Atmosphere (GLORIA) scientific objectives, Atmos. Meas. Tech. Discuss., 7, 1535–1572, doi:10.5194/amtd-7-1535-2014, 2014. 4232, 4233

Rothman, L., Gordon, I., Babikov, Y., Barbe, A., Benner, D. C., Bernath, P., Birk, M., Bizzocchi, L., Boudon, V., Brown, L., Campargue, A., Chance, K., Cohen, E., Coudert, L., Devi, V., Drouin, B., Fayt, A., Flaud, J.-M., Gamache, R., Harrison, J., Hartmann, J.-M., Hill, C., Hodges, J., Jacquemart, D., Jolly, A., Lamouroux, J., Roy, R. L., Li, G., Long, D., Lyulin, O., Mackie, C., Massie, S., Mikhailenko, S., Müller, H., Naumenko, O., Nikitin, A., Orphal, J., Perevalov, V., Perrin, A., Polovtseva, E., Richard, C., Smith, M., Starikova, E., Sung, K., Tashkun, S., Tennyson, J., Toon, G., Tyuterev, V., and Wagner, G.: The HITRAN2012 molecular spectroscopic database, J. Quant. Spectrosc. Ra., 130, 4–50, 2013. 4236

Seo, K.-H. and Bowman, K. P.: Lagrangian estimate of global stratosphere-troposphere mass exchange, J. Geophys. Res.-Atmos., 107, ACL2-1–ACL2-8, 2002. 4231

Solomon, S., Qin, D., Manning, M., Alley, R., Berntsen, T., Bindoff, N., Chen, Z., Chidthaisong, A., Gregory, J., Hegerl, G., Heimann, M., Hewitson, B., Hoskins, B., Joos, F., Jouzel, J., Kattsov, V., Lohmann, U., Matsuno, T., Molina, M., Nicholls, N., Overpeck, J., Raga, G., Ramaswamy, V., Ren, J., Rusticucci, M., Somerville, R., Stocker, T., Whetton, P., Wood, R. A., and Wratt, D.: Technical summary, in: Climate Change 2007 – The Physical Science Basis, Contribution of Working Group I to the Fourth Assessment Report of the Intergovernmental Panel on Climate Change, available at: http://www.ipcc.ch/pdf/assessment-report/ar4/wg1/ar4-wg1-ts.pdf, 19–91, Cambridge University Press, Cambridge, UK and New York, NY, USA, 2007. 4231

Spang, R., Remedios, J. J., and Barkley, M. P.: Colour indices for the detection and differentiation of cloud type in infra-red limb emission spectra, Adv. Space Res., 33, 1041–1047, 2004. 4247

Twomey, S.: Introduction to the Mathematics of Inversion in Remote Sensing and Indirect Measurements, Dover Publications, Mineola, NY 11501, USA, 1977. 4237

Ungermann, J., Kaufmann, M., Hoffmann, L., Preusse, P., Oelhaf, H., Friedl-Vallon, F., and Riese, M.: Towards a 3-D tomographic retrieval for the air-borne limb-imager GLORIA, Atmos. Meas. Tech., 3, 1647–1665, doi:10.5194/amt-3-1647-2010, 2010. 4232, 4248

Ungermann, J., Blank, J., Lotz, J., Leppkes, K., Hoffmann, L., Guggenmoser, T., Kaufmann, M., Preusse, P., Naumann, U., and Riese, M.: A 3-D tomographic retrieval approach with advection compensation for the air-borne limb-imager GLORIA, Atmos. Meas. Tech., 4, 2509–2529, doi:10.5194/amt-4-2509-2011, 2011. 4236

Ungermann, J., Pan, L. L., Kalicinsky, C., Olschewski, F., Knieling, P., Blank, J., Weigel, K., Guggenmoser, T., Stroh, F., Hoffmann, L., and Riese, M.: Filamentary structure in chemical tracer distributions near the subtropical jet following a wave breaking event, Atmos. Chem. Phys., 13, 10517–10534, doi:10.5194/acp-13-10517-2013, 2013. 4232, 4236

Vogel, B., Günther, G., Grooß, J.-U., and Müller, R.: Eastward eddy shedding from the asian monsoon anticyclone and associated transport pathways of boundary layer sources to the stratosphere in September 2012, Atmos. Chem. Phys. Discuss., in preparation, 2014. 4243

Volk, C. M., Riediger, O., Strunk, M., Schmidt, U., Ravegnani, F., Ulanovsky, A., and Rudakov, V.: In situ tracer measurements in the tropical tropopause region during APE-THESEO, Eur. Comm. Air Pollut. Res. Report, 73, 661–664, 2000. 4243

von Clarmann, T. and Echle, G.: Selection of optimized microwindows for atmospheric spectroscopy, Appl. Optics, 37, 7661–7669, 1998. 4241

von Clarmann, T., Höpfner, M., Kellmann, S., Linden, A., Chauhan, S., Funke, B., Grabowski, U., Glatthor, N., Kiefer, M., Schieferdecker, T., Stiller, G. P., and Versick, S.: Retrieval of temperature, H_2O, O_3, HNO_3, CH_4, N_2O, $ClONO_2$ and ClO from MIPAS reduced resolution nominal mode limb emission measurements, Atmos. Meas. Tech., 2, 159–175, doi:10.5194/amt-2-159-2009, 2009. 4243

Weigel, K., Hoffmann, L., Günther, G., Khosrawi, F., Olschewski, F., Preusse, P., Spang, R., Stroh, F., and Riese, M.: A stratospheric intrusion at the subtropical jet over the Mediterranean Sea: air-borne remote sensing observations and model results, Atmos. Chem. Phys., 12, 8423–8438, doi:10.5194/acp-12-8423-2012, 2012. 4232

Werner, A., Volk, C. M., Ivanova, E. V., Wetter, T., Schiller, C., Schlager, H., and Konopka, P.: Quantifying transport into the Arctic lowermost stratosphere, Atmos. Chem. Phys., 10, 11623–11639, doi:10.5194/acp-10-11623-2010, 2010. 4243

Woiwode, W., Oelhaf, H., Gulde, T., Piesch, C., Maucher, G., Ebersoldt, A., Keim, C., Höpfner, M., Khaykin, S., Ravegnani, F., Ulanovsky, A. E., Volk, C. M., Hösen, E., Dörnbrack, A., Ungermann, J., Kalicinsky, C., and Orphal, J.: MIPAS-STR measurements in the Arctic UTLS in winter/spring 2010: instrument characterization, retrieval and validation, Atmos. Meas. Tech., 5, 1205–1228, doi:10.5194/amt-5-1205-2012, 2012. 4232, 4243

Woiwode, W., Suminska-Ebersoldt, O., Oelhaf, H., Höpfner, M., Ebersoldt, A., Friedl-Vallon, F., Gulde, T., Kaufmann, M., Kleinert, A., Krömer, M., T. Kulessa, G. M., Piesch, C., Riese, M., Rongen, H., Sartorius, C., Schardt, G., Schönfeld, A., Schuettemeyer, D., Stroh, F., Volk, C. M., and Orphal, J.: Validation of first chemistry mode retrieval results from new imaging FTIR spectrometer GLORIA with correlative MIPAS-STR observations, Atmos. Meas. Tech. Discuss., in preparation, 2014. 4234

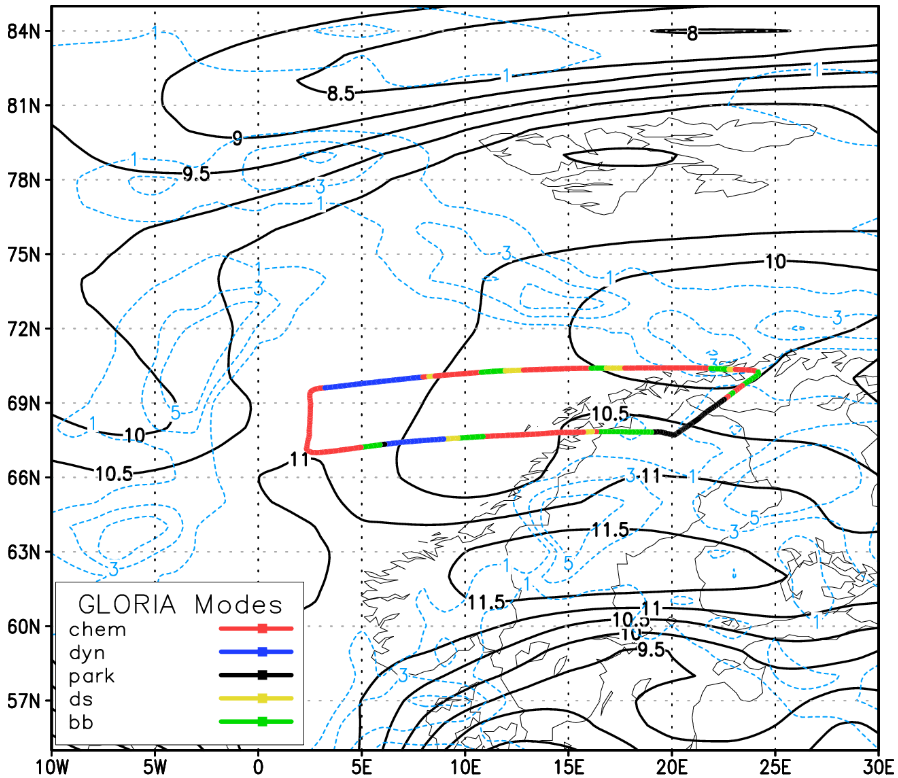

Fig. 1. Potential vorticity (in PVU, black solid lines) on 370 K isentropic surface (at approx. flight level) and cirrus clouds in lower levels (shown by cloud ice water content [10^5 kg kg^{-1}] on 280 K, blue lines) and the track of the Geophysica aircraft for ESSenCe Flight 2 of 16 December 2011. "dyn" and "chem" mark dynamics and chemistry mode measurements of GLORIA, respectively. "park" indicates that GLORIA is in parking position, "ds" and "bb" indicate deep space and blackbody calibration measurements, respectively.

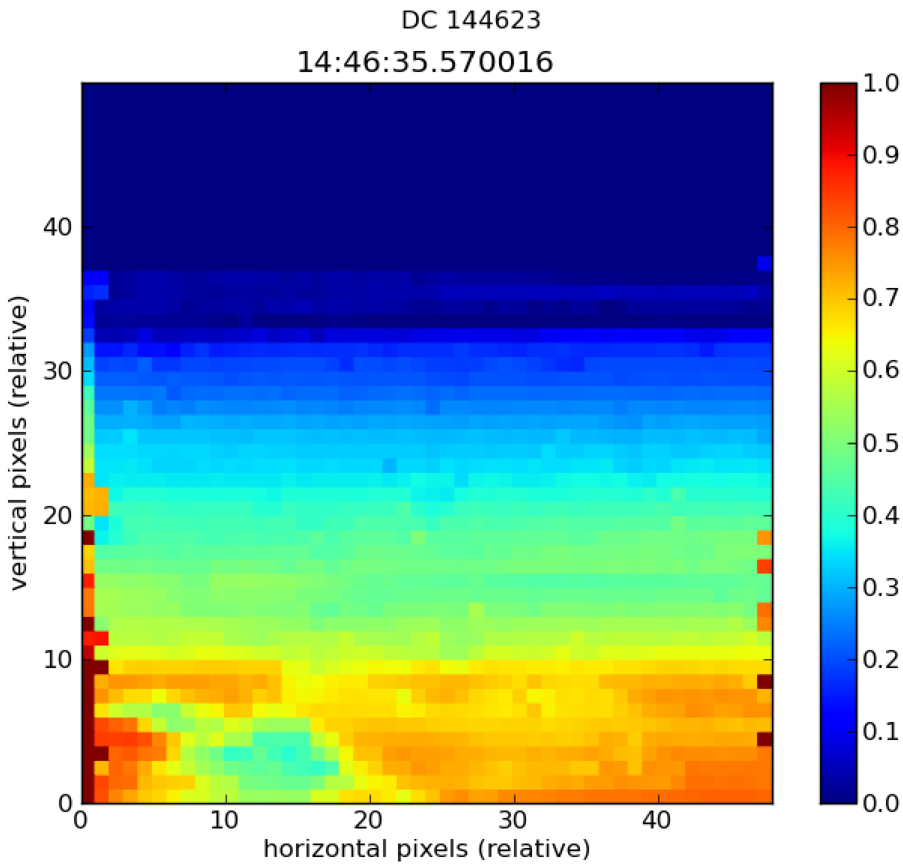

Fig. 2. Direct current signal (arb. units) for one GLORIA image, before the Fourier transformation is applied. Exposure time is 40 ms and the horizontal extent is about 7.5 km at 10 km tangent altitude.

AMTD
7, 4229–4274, 2014

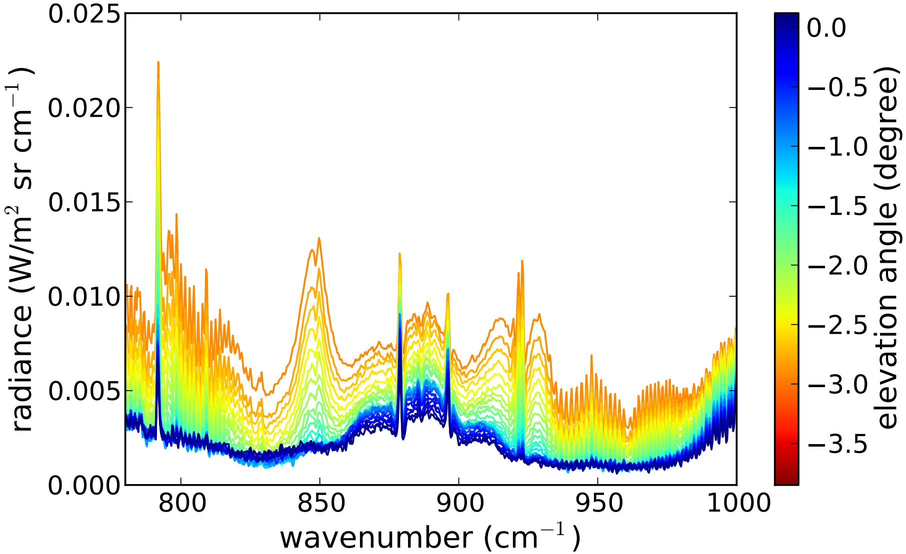

Fig. 3. Spectra obtained by averaging over a detector row for a single GLORIA dynamics mode measurement (Image 72, measured at 15:04:49 UTC at 67° N, 7° E) after pixel weighting and filtering. Corresponding tangent altitudes are 9 km (red) to 15 km (dark blue).

AMTD
7, 4229–4274, 2014

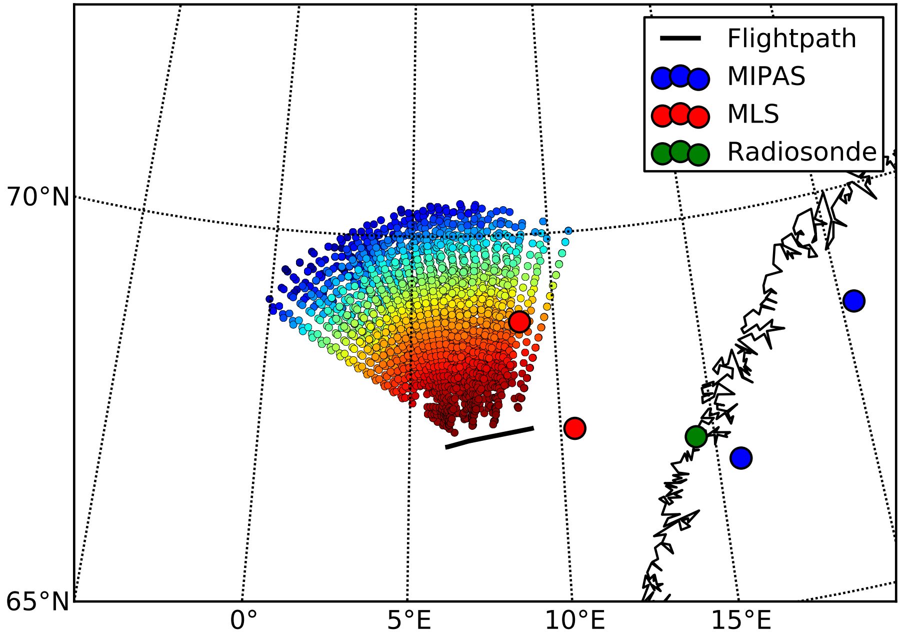

Fig. 4. GLORIA tangent points of dynamics mode measurements during ESSenCe Flight 2. Tangent points closest (furthest) from the flight path (black line) are at highest (lowest) altitudes. Corresponding tangent altitudes are 4 km (red) to 15 km (blue). Thick colored dots mark the geolocation of collocated MIPAS-Envisat and EOS-MLS tangent points and radiosonde positions. MIPAS-Envisat measurements were made on 16 December 2011 at 15:21 and 16:09 UTC, and EOS-MLS measurements at 11:40 and 11:42, respectively.

AMTD
7, 4229–4274, 2014

Retrieval of three-dimensional small scale structures

M. Kaufmann et al.

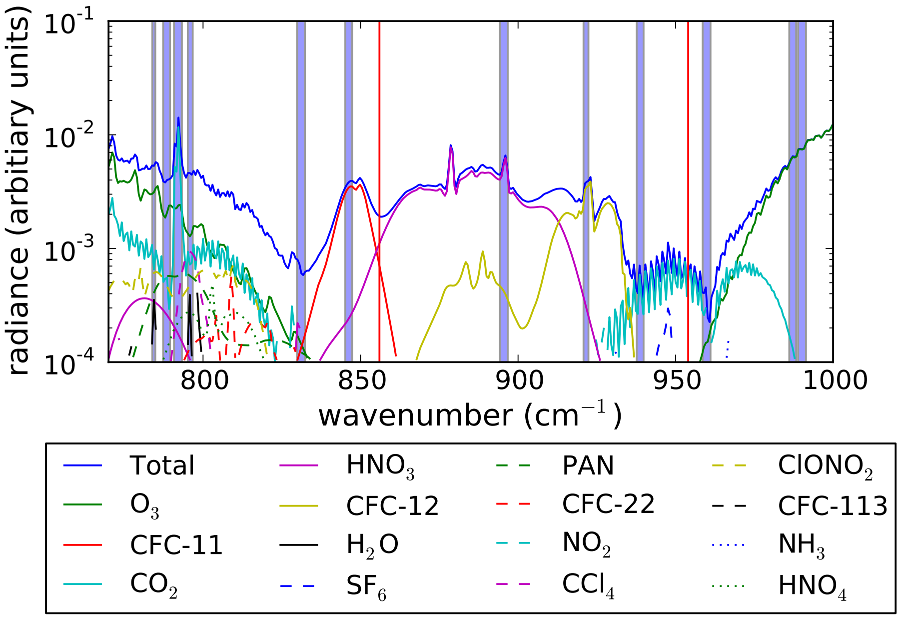

Fig. 5. Simulated GLORIA dynamics mode spectra for 16 km tangent altitude applying the MIPAS reference atmosphere for mid latitudes. The spectral windows utilized in the retrieval are marked by blue vertical boxes.

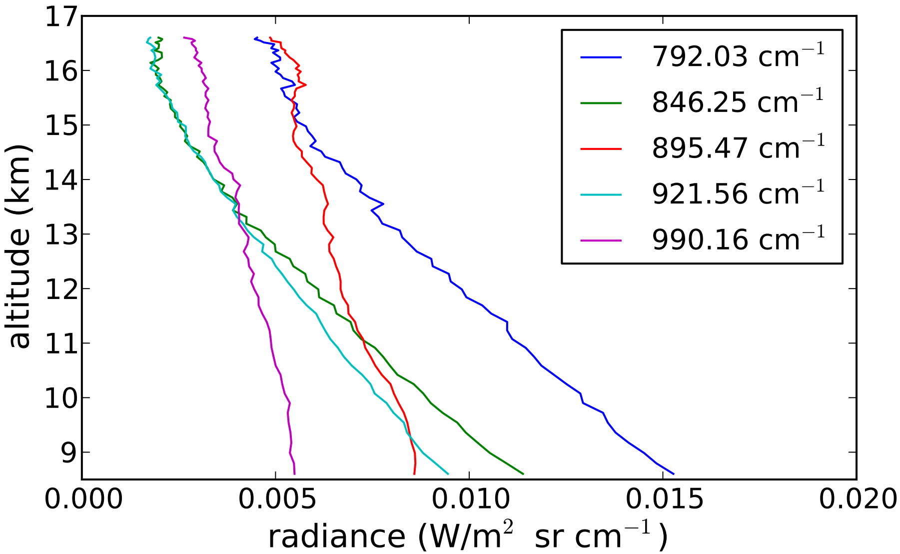

Fig. 6. GLORIA integrated radiances for some spectral windows as selected by the genetic algorithm. The data is for Image 72 at 67° N and 7° E on 16 December, 15:05 UTC.

AMTD
7, 4229–4274, 2014

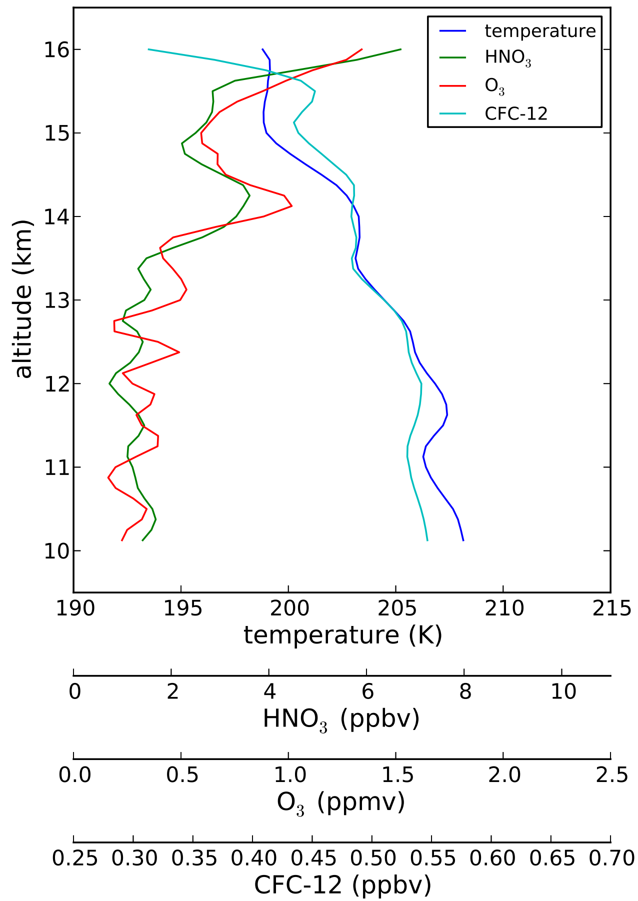

Fig. 7. Retrieved temperature, HNO_3, O_3 and CFC-12 for GLORIA Image 72.

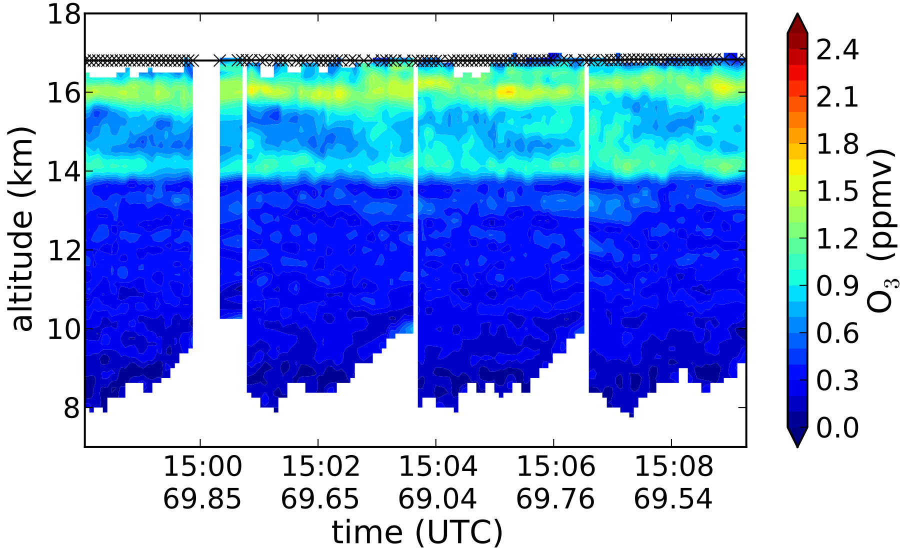

Fig. 8. Retrieved ozone volume mixing ratio from GLORIA dynamics mode data for 16 December 2011. Universal time and geographic latitude (in degrees) label the *x* axis. The figure shows four horizontal sweeps starting at 48° and ending at 118° with respect to the airplane nose.

AMTD
7, 4229–4274, 2014

Retrieval of three-dimensional small scale structures

M. Kaufmann et al.

Title Page
Abstract
Introduction
Conclusions
References
Tables
Figures
◀▶
Back
Close
Full Screen / Esc
Printer-friendly Version
Interactive Discussion

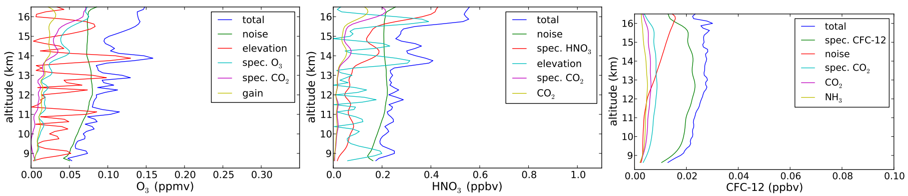

Fig. 9. Error budget for HNO_3, O_3 and CFC-12 for GLORIA Image 72.

AMTD
7, 4229–4274, 2014

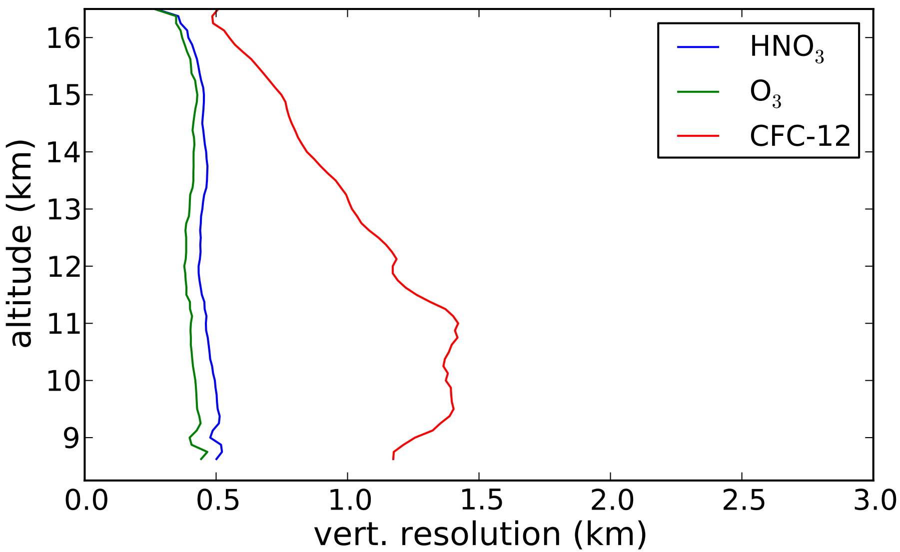

Fig. 10. Vertical resolution for HNO_3, O_3 and CFC-12, for GLORIA Image 72.

AMTD

7, 4229–4274, 2014

Retrieval of three-dimensional small scale structures

M. Kaufmann et al.

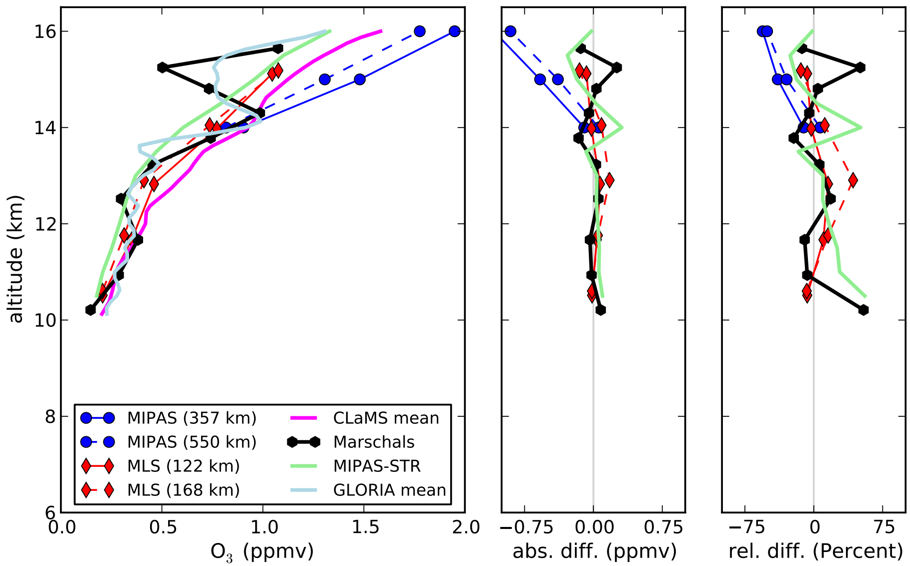

Fig. 11. Comparison of O_3 abundance between GLORIA dynamics mode measurements and various collocated datasets.

AMTD
7, 4229–4274, 2014

Retrieval of three-dimensional small scale structures

M. Kaufmann et al.

Title Page
Abstract Introduction
Conclusions References
Tables Figures
◀◀ ▶▶
◀ ▶
Back Close
Full Screen / Esc
Printer-friendly Version
Interactive Discussion

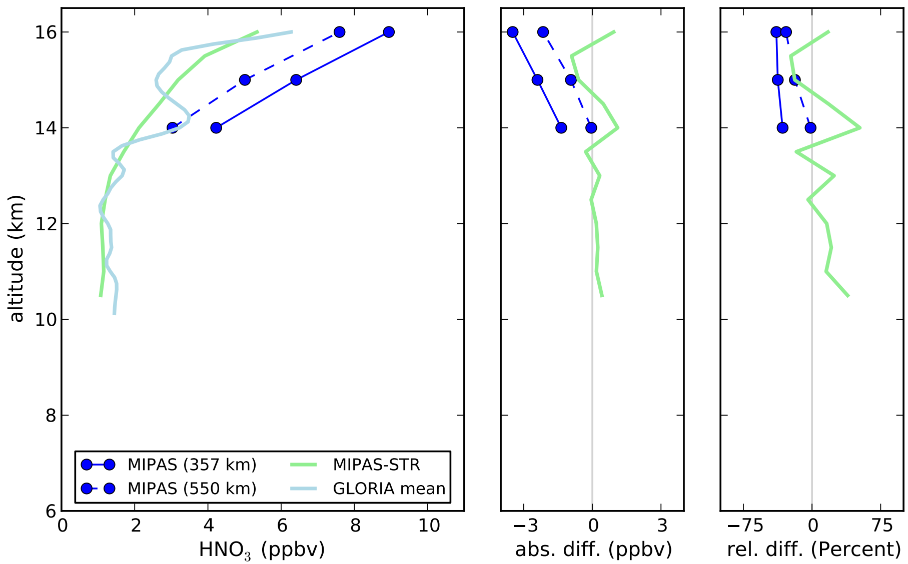

Fig. 12. Comparison of HNO_3 abundance between GLORIA dynamics mode measurements and collocated datasets.

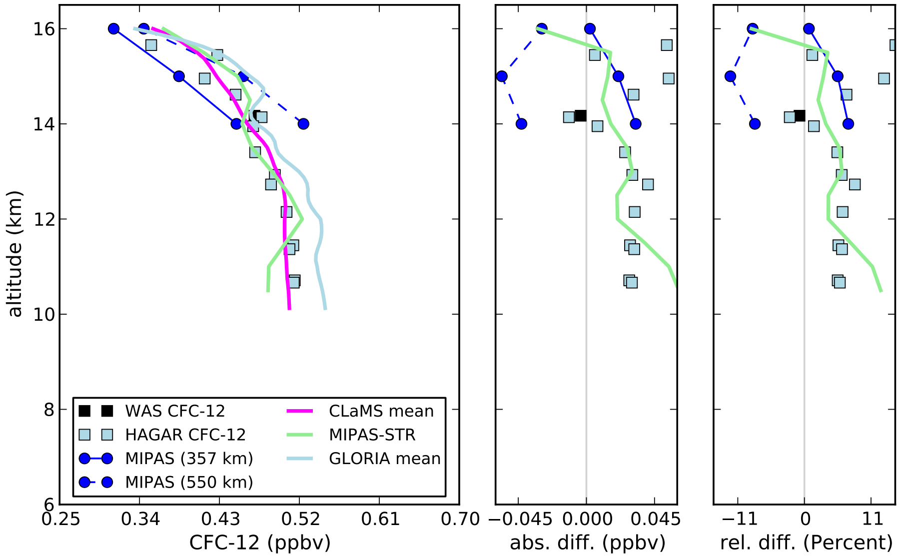

Fig. 13. Comparison of CFC-12 abundance between GLORIA dynamics mode measurements and collocated datasets.

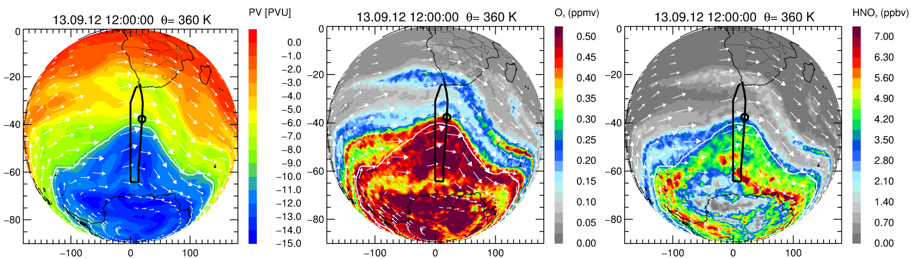

Fig. 14. ECMWF potential vorticity (left) at a potential temperature of 360 K (about 12 km altitude) for the TACTS/ESMVal flight on 13 September 2012. The flight track is indicated by a black line. At 45° S, 20° E a tomographic flight pattern (approx. altitude about 12.5 km) was performed. The middle and right plots show O_3 and HNO_3 volume mixing ratios at 360 K as simulated by the CLaMS model, respectively. The vortex edge is calculated as defined by Nash et al. (1996) and is marked by a white contour line. The horizontal winds are indicated by white arrows.

AMTD
7, 4229–4274, 2014

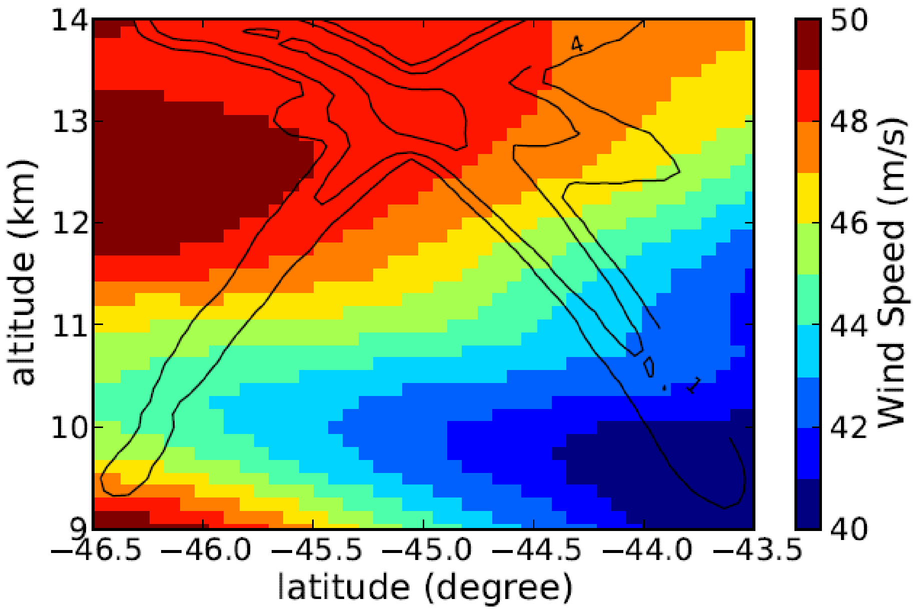

Fig. 15. Horizontal wind speeds at 20° E for 13 September 2012, 14:00 UTC. Contour lines (at 2, 4, 16) indicate the number of tangent points per grid cell; highest numbers are at the center of the plot.

AMTD
7, 4229–4274, 2014

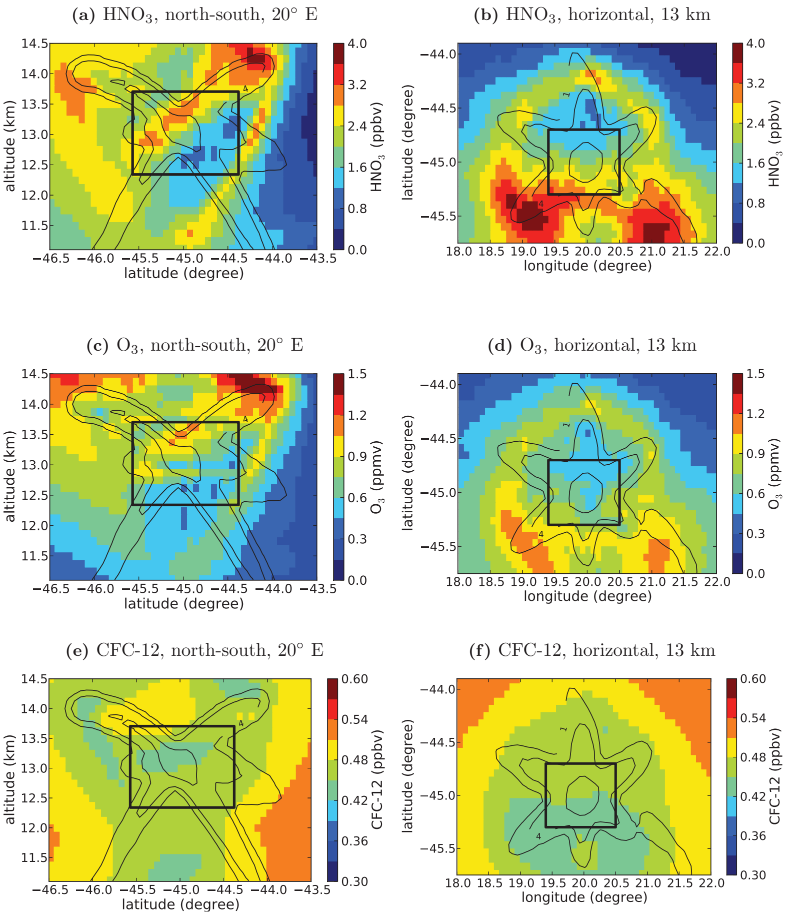

Fig. 16. Retrieved HNO_3, O_3 and CFC-12 mixing ratios at 20° E (left) and 13 km altitude (right) for 13:30–14:30 UTC, 13 September 2012. Contour lines (at 2, 4, 16) indicate the number of tangent points per grid cell; highest numbers are at the center of the plot.

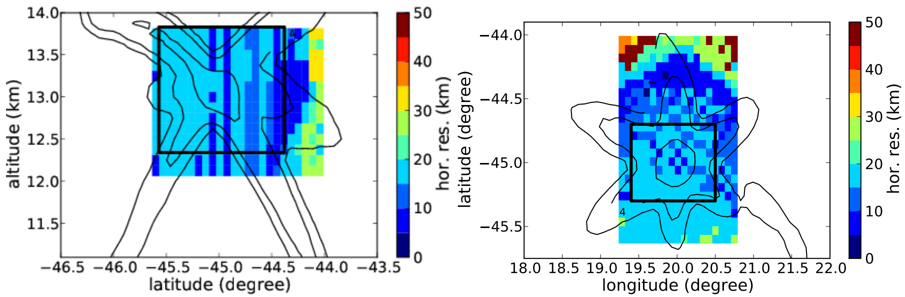

Fig. 17. HNO_3 horizontal resolution at 20° E (left) and 13 km altitude (right). Contour lines (at 2, 4, 16) indicate the number of tangent points per grid cell; highest numbers are at the center of the plot.

AMTD
7, 4229–4274, 2014

Retrieval of three-dimensional small scale structures

M. Kaufmann et al.

Title Page
Abstract Introduction
Conclusions References
Tables Figures
Back Close
Full Screen / Esc
Printer-friendly Version
Interactive Discussion

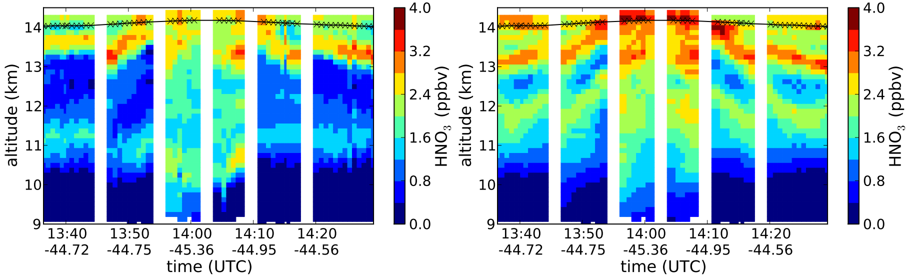

Fig. 18. Comparison between a one-dimensional (left) and three-dimensional (right) reconstruction of HNO_3 during the GLORIA hexagonal flight. The segments of the hexagon are separated by white stripes. Measurement time (UTC) and latitude (deg) for the beginning of each segment are given on the *x* axis.